Electrocatalytic Reduction Mechanisms of CO_2 on MoS_2 Edges Using Grand-Canonical DFT: From CO_2 Adsorption to HCOOH or CO

Muhammad Akif Ramzan, Rémi Favre, Stephan N. Steinmann, Tangui Le Bahers, Pascal Raybaud

Electrocatalytic Reduction Mechanisms of CO_2 on MoS_2 Edges using Grand-canonical DFT: from CO_2 Adsorption to HCOOH or CO

Muhammad Akif Ramzan,[†] Rémi Favre,[‡] Stephan N. Steinmann,[*,‡] Tangui Le Bahers,[*,‡,¶] and Pascal Raybaud[*,†,‡]

†*IFP Energies nouvelles, Rond-point de l'échangeur de Solaize - BP 3 69360 Solaize - France*

‡*CNRS, Laboratoire de Chimie UMR 5182, ENS de Lyon, 46 allée d'Italie, Lyon F-69342, France*

¶*Institut Universitaire de France, 5 rue Descartes, 75005 Paris, France*

E-mail: stephan.steinmann@ens-lyon.fr; tangui.le_bahers@ens-lyon.fr; pascal.raybaud@ifpen.fr

Abstract

Efficiently converting carbon dioxide (CO_2) into valuable fuels or chemicals represents one of the great challenges at the core of current scientific researches. Here, we report a DFT-based theoretical study of the reactivity of two main MoS_2 edges for electrocatalytic, or eventually photocatalytic, reduction of CO_2. By explicitly accounting for the electrode potential via a grand-canonical ensemble that controls the number of electrons, we show that the two edges exhibit different H coverage which, in turn, directly influences the CO_2-reduction energy profile under relevant reducing potentials. Specifically, on S-edge, a 0.375 ML H coverage enables the CO_2 activation through its adsorption in a bidentate mode with a limiting potential of 0.07 V vs. SHE. By contrast, H coverage on Mo-edge at reducing potentials relevant for CO_2 reduction was determined to be 0 ML. On this bare Mo-edge, CO_2 activation occurs at an additional energy cost of 0.44 eV for -0.80 V. Consequently, the activated CO_2 on S-edge exhibits comparable and thermodynamically favorable reactivity for the two possible two-electron products, formic acid and carbon monoxide (CO), with limiting potentials of -0.54 V and -0.34 V, respectively. The two products, however, show different desorption behavior with CO desorption being endergonic and independent of electrode potential. Conversely, the reactivity of Mo-edge is less favored and it is anticipated to favor formic acid over CO due to a highly endergonic $C-O$ bond-breaking step in the adsorbed COOH intermediate. This step was determined to be exergonic on S-edge. This study paves the way for a better understanding of CO_2 reduction mechanisms on MoS_2 edges and highlights the key role of the CO_2 adsorption step which was generally neglected in prior investigations.

1 Introduction

Reducing drastically carbon dioxide (CO_2) emissions represents nowadays one of the most urgent challenges to tackle. This crucial concern has prompted our society to transition from a fossil resources-based economy to a more environmentally friendly and carbon-neutral one, anchored in the utilization of energy derived exclusively from renewable sources.[1–3] At the same time, assuming that CO_2 can be captured in the exhaust gas emitted from industrial plants, its catalytic conversion to fuels or chemicals could be a profitable endeavor.[4] Various potential ways to realize efficiently this conversion are investigated nowdays, but we are still far from the optimal operating point. Sunlight, a pivotal and almost unlimited renewable energy source, could play a central role in driving this transformation, either indirectly via initial production of electricity which, in turn, can drive the electrocatalytic reduction (hydrogenation) of CO_2[5,6] or directly through a photocatalytical pathway.[7,8] The former pathway requires the use of metallic active phases in order to activate CO_2 through successive coupled transfers of electrons and protons. The latter pathway, sometimes referred to as artificial photosynthesis,[9,10] requires the use of a light-harvesting material to convert light into electron-hole pairs which subsequently carry out the oxidation-reduction half reactions at the surface of a suitable (co-)catalyst.
However, currently known electro- or photo-catalysts suffer from low reactivity, selectivity and require to be further optimized in order to become industrially usable.

Molybdenum disulfide (MoS_2), a prominent member of the 2D transition-metal dichalcogenides (TMDCs) family and renowned for its versatile roles as catalyst of various chemical processes such as hydrotreatment of petroleum cuts or biomass conversion[11,12] has recently shown promise for various electro- and photo-catalytic applications. In particular, the electrochemical hydrogen evolution reaction (HER)[13,14] and the CO_2 photoreduction could be catalysed by MoS_2.[15,16] As an example, Asadi et al. demonstrated high efficiency of MoS_2 for electrochemical reduction of CO_2, outperforming noble metals, particularly at its Mo-

terminated edges.[17] They showcased a high current density for carbon monoxide (CO) formation at low overpotential in an ionic liquid, which was also deemed responsible for the observed suppression of the competing HER, as also shown previously.[18] Furthermore, based on density functional theory (DFT) calculations,,[19] heterojunctions of MoS_2 with semiconducting materials, like TiO_2, have been proposed to exhibit type II or Z-scheme formalisms, favorable for photocatalytic reduction of CO_2. Similar heterojunctions have recently been realized experimentally and exhibited CO or CH_4 product selectivity as a function of the light wavelength.[20]

DFT-based computational studies have proved tremendously useful in not only elucidating the experimental observations on known materials but also guiding the experiments towards novel materials with enhanced catalytic efficiency.[13] Using the frequently used computational hydrogen electrode (CHE) approach,[21,22] Nørskov's group demonstrated that (doped-)edges of TMDCs deviate from a linear relationship between the binding strength of various key intermediates, mainly because they offer two distinct sites for adsorption of reaction species.[23,24] Such linear scaling relations were previously shown to be characteristic of transition metal catalysts and a major contributor to their inherent inefficiency.[25] Furthermore, same group identified the d-band center as a universal descriptor of edge structure and adsorption strength of reaction species on MoS_2 edges.[26] Another DFT study explored the optimal dopants in MoS_2 for CO_2-reduction electrocatalysis, identifying V, Zr, and Hf as effective dopants that enhance CO desorption from the MoS_2 edge.[27] More recently, edge configurations, adsorption properties and aqueous stability of various TMDCs was investigated in a CHE-based study which revealed material-specific preferences for stable edge configurations and varying linear scaling relations among sulfides, selenides, and tellurides.[28] In addition, defect engineering, particularly the introduction of grain boundaries with S-vacancies located on the basal plane, is predicted by DFT calculations to be a promising strategy for activating the largely-exposed but inert basal plane of MoS_2 for CO_2 electrochemical reduction.[29]

However, to the best of our knowledge, none of these studies has been directed towards elucidating the inherent reactivity of pristine MoS_2 for CO_2 (photo-)electroreduction, with an explicit consideration of the electrode potential inducing an explicit surface charging effect. In particular, the question of CO_2 molecular adsorption which is a precursor state of its activation on MoS_2 edges remains elusive in most of the reported DFT-based studies, mainly because the CHE approach is only suited for the proton-coupled-electron-transfer (PCET) electrochemical steps and can not handle the effect of electrode potential on the chemical nature of the adsorbed states. Hence, in most of the aforementioned works, the first PCET is assumed to occur prior or simultaneously to CO_2-adsorption process directly leading to COOH* or OCHO* as first adsorbed intermediates. As has been discussed in an ample amount of literature for many years,[8,30] it is of paramount importance to analyze whether the formation of a negatively charged CO_2 is thermodynamically possible on the MoS_2 sites under reasonable electrode potential, and if the adsorption mode (through either carbon, or oxygen or mixed carbon-oxygen coordination) on the molybdenum and/or sulfur site(s) may induce the disruption of the molecular linearity and activate the first PCET. In addition, the criteria of the competition between CO_2-reduction and HER, which is deemed to be the prevalent transformation under CO_2-reduction conditions,[31] have not been explicitly determined. Using grand-canonical DFT to explicitly account for the electrode potential, we here fill this gap by first ascertaining the state of the MoS_2 edges under aqueous (acidic) conditions, and then studying the reaction free energy profile for the formation of the two-electron products potentially resulting from CO_2 reduction, namely CO and formic acid (HCOOH). In particular, we will pay particular attention on the CO_2 adsorption step as a function of edge sites, H coverages and electrode potential.

2 Methods

Periodic, plane-waves-based DFT as implemented in the Vienna Ab initio Simulation Package (VASP)[32] was used to carry out all the simulations. The energies of the valence electrons were approximated at the GGA level using the Perdew-Burke-Ernzerhof (PBE)[33] exchange-correlation functional with the plane-wave basis set truncated at 500 eV. The exchange-correlation energies were further augmented by the dispersion correction of Grimme with a Becke-Johnson damping function.[34,35] The core electrons and the nuclei were treated under the Projector Augmented Wave (PAW) approximation.[36,37] To sample the Brillouin zone a 3×3×1 Gamma-centered k-point grid was used. Convergence of self-consistency cycles was achieved up to a minimum of 1.0×10^{-5} eV and the partial occupancies of the orbitals were determined via the physically-motivated Fermi function at room temperature (0.025 eV). All degrees of freedom were relaxed during optimization until the magnitude of force on each atom was below 0.025 eV/Å.

The so-called slab model was used to simulate the MoS_2 edges. A symmetric p(4×5) supercell exposing, simultaneously, both Mo-/S-terminated edges was constructed by cleaving the fully-optimized 2H-bulk (a = b = 3.15 Å, c = 12.08 Å) structure along (100) lattice direction, and making use of point symmetry between two MoS_2 layers (Figure 1). The symmetric, two-layered supercell allows to avoid the expensive dipole corrections to force and energy which are otherwise needed for an accurate estimation of the work function of the slab systems. Furthermore, this model corresponds to multilayered MoS_2 particles which are also relevant experimentally. We chose a 4-Mo atoms wide edge model in order to accommodate a large number of possible intermediates. As discussed in Ref.,[38] this choice may impact the reconstruction of the Mo-edge. In the present case, we observe a clustering of 2 Mo atoms (Figure S6) whereas for a 3-Mo atoms edge model, the clustering involves 3 atoms. In the real catalyst, MoS_2 particles expose edges of various finite lengths which may induce a mixture of both types of reconstruction. Each edge contained 50 % S coverage, which

was previously estimated to be the most stable edge configuration,[39] especially under sulfur deficient conditions, and leads to a stoichiometric MoS_2-slab structure. Large enough ($\approx$ 20 Å on each side) vacuum was introduced in the normal direction to preclude interactions with the periodic images. All the surface species were adsorbed in a symmetric fashion on the top and bottom edges to avoid a net dipole moment across the cell. However, for sake of convenience, in the following we discuss energies related to *half* of the system i.e. adsorption of one hydrogen atom is taken as half of the adsorption energy of one hydrogen on top and one on the bottom of the slab.

The effect of the electrode potential was modeled via grand-canonical DFT (GC-DFT)[40]

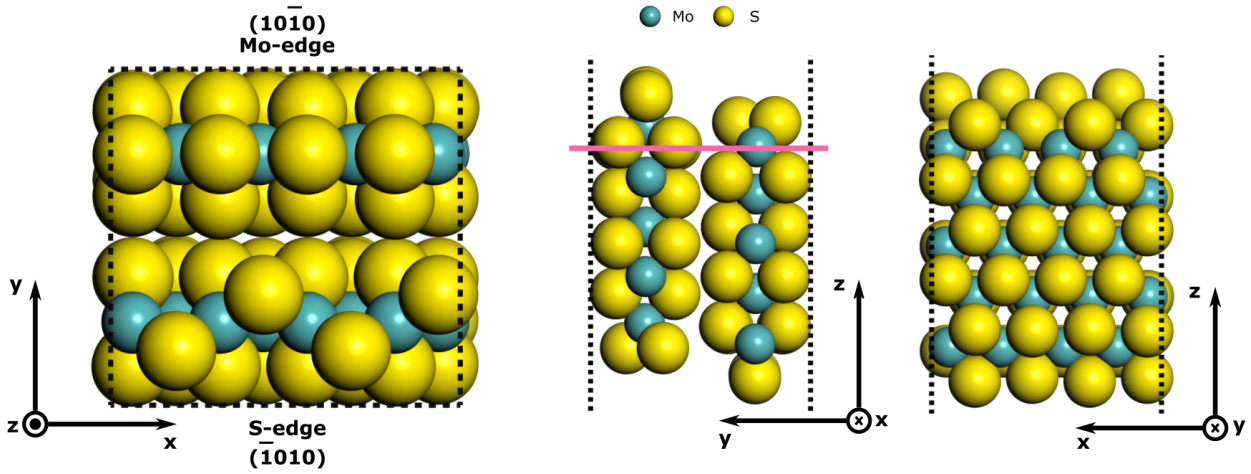

Figure 1: p(4×5) slab-like supercell adopted in this study to simulate MoS_2 edges at 50 % S coverage. The supercell was symmetrized using the inversion center (C_s point group) between two MoS_2 layers. All the atoms below the pink line were kept fixed during the frequency calculations.

using the surface charging approach as described in Ref.[41] An implicit electrolyte model involving the self-consistent solution of the linearized Poisson-Boltzmann equation,[42,43] implemented in VASP as VASPsol,[44] was employed using the same parameters previously optimized for MoS_2.[41]

The potential-dependent electronic energies of the surface species were augmented by en-

thalpic and entropic contributions to the free energy under harmonic approximation at 298.15 K. This was achieved via a frequency calculation of the adsorbates and a part of the surface (Figure 1) in the fully-optimized, zero charged geometry. The non-symmetric enthalpic and entropic contributions thus calculated were added to the energy of the *half* of the system, as described above. The gas phase species were optimized in a 20 Å cubic box at the Gamma point. The gas phase energies include the appropriate translational, rotational and vibrational entropy and enthalpy contributions corresponding to 1 atm and 298.15 K under the rigid-rotor, ideal-gas approximation. In particular, the entropy contribution of H_2O was divided by two to reflect the liquid state.[45,46] All reported electrode potentials are referenced to the standard hydrogen electrode (SHE), whose potential was set to 4.44 V vs. vacuum as recommended by IUPAC.[47] Acidic conditions were assumed throughout by setting pH=0.

3 Results and Discussion

3.1 Hydrogenation of the edges

Since HER is a prominent side reaction occurring along with CO_2 reduction,[31] we have studied various coverages of H on both Mo and S edges in order to determine the equilibrium H coverage on each edge. In the following, the H coverage is defined as fraction of a monolayer given by

$$\Theta_{\mathrm{H}}(\mathrm{ML}) = \frac{\mathrm{n_H}}{2\mathrm{n_{Mo}}}, \tag{1}$$

where $\mathrm{n_H}$ is the number of H atoms adsorbed at the given edge and $\mathrm{n_{Mo}}$ is the number of edge-most Mo atoms present on the same edge, i.e., four in our case. We have studied all coverages of 0-1 ML in steps of 0.125. At each coverage, the most stable configuration of H atoms was determined by checking all possibilities of adding one H to the previously found most-stable configuration.

As is a well-known fact, the HER is governed by the combination of adsorption of H via so-called Volmer step and the evolution of H_2 via so-called Heyrovsky or Tafel steps. We find that Tafel reaction is always endergonic on MoS_2 edges, thereby making Heyrovsky the most likely mechanism for H_2 evolution at all coverages and electrode potentials, in line with previous studies.[48] As such, in our case HER is governed by the combination of the following two reactions

$$\Delta G_{Vol}: \ nH^* + \left(H^+ + e^-\right) \rightarrow (n+1)H^*$$

$$\Delta G_{Hey}: \ nH^* + \left(H^+ + e^-\right) \rightarrow (n-1)H^* + H_2,$$

which, respectively, denote Volmer and Heyrovsky reaction steps with corresponding reaction free energies, ΔG_{Vol} and ΔG_{Hey}.

3.1.1 S-edge

In Supplementry Information (SI) we give full details regarding the adsorption behavior of H on two edges at various coverages and plot the corresponding Volmer and Heyrovsky reaction free energies as a function of potential and coverage. Here we give but a mere summary of the results important for the ensuing discussion of the CO_2 reduction on the two edges. On S-edge we could differentiate two zones of interest: (i) at mild reducing potentials, i.e. up to -0.4 V, the equilibrium coverage is 0.5 ML both thermodynamically and kinetically and (ii) at highly reducing potentials, 0.5 ML is still the equilibrium coverage and the higher potential simply leads to the evolution of any additional H that could adsorb on the surface, thanks to a very exergonic Heyrovsky step. This 0.5 ML equilibrium coverage of H on S-edge was previously determined in a heuristic fashion by Chan et al. in the context of CO_2 electroreduction.[23] However, they considered S-edge at 100 % S coverage which is not the chemically most relevant system in light of the recent theoretical studies which show that low S-coverage is not only reachable but also more stable under electrochemical conditions.[28]

Furthermore, we notice, in agreement with Ref.,[23] that the ΔG_{Vol} at 0.375 ML and ΔG_{Hey} at 0.5 ML are very similar (Figure 2). Hence, we cannot exclude the possibility that a coverage of 0.375 ML is accessible, and real steady-state coverage could be between 0.375 ML and 0.5 ML. Note that the 0.375 ML coverage will become more relevant when we discuss the reactivity of CO_2 electroreduction.

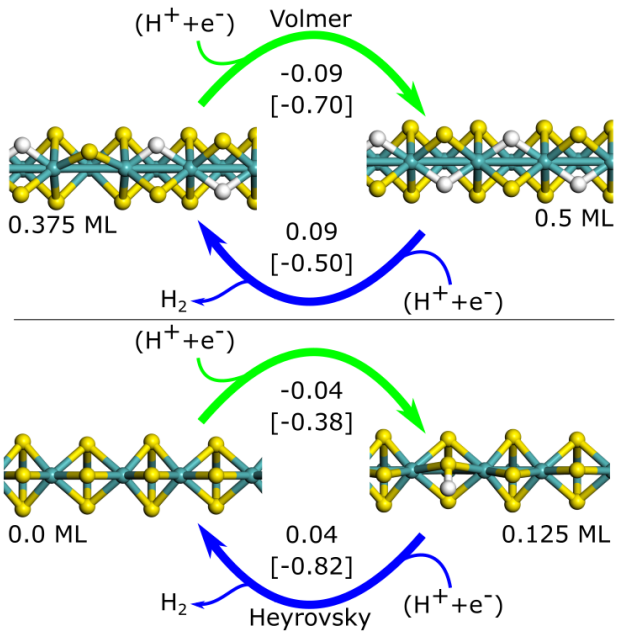

Figure 2: Relevant Volmer and Heyrovsky reaction free energies on (top) S-edge and (bottom) Mo-edge at 0.0 V and -0.6 V (the value in brackets). The atomic structures correspond to the most-stable H-adsorption configurations at the coverages mentioned.

3.1.2 Mo-edge

On Mo-edge, the Heyrovsky step is always more exergonic than Volmer at non-zero coverages. This signigies that the equilibrium H coverage on this edge is essentially 0.0 ML. The Volmer step involving the adsorption of first H and the corresponding Heyrovsky step for it's evolution have been depicted in Figure 2 along with their reaction free energies at two relevant potentials. At potentials relevant for CO_2 electroreduction, this Heyrovksy step is

much more exergonic and thus, the coverage of H is considered to be 0.0 ML on this edge for all subsequent discussion of reactivity. Notably, the small 0.125 ML coverage can only be stabilized in a small potential window of less reducing that -0.1 V (Figure S5(b)).

3.2 Reduction of CO_2 on Mo/S-edges

Photo- or electro-chemical reduction of CO_2 into HCOOH or CO is a two-electron, two-proton transformation governed by the following equations

$$CO_2 + 2H^+ + 2e^- \rightarrow HCOOH \qquad E^o = -0.20\ V\ \ (-0.18\ V) \tag{2}$$

$$CO_2 + 2H^+ + 2e^- \rightarrow CO + H_2O \qquad E^o = -0.12\ V\ \ (-0.52\ V), \tag{3}$$

where E^o is the experimentally determined standard electrochemical potential at equilibrium. The values in parenthesis are the calculated equilibrium potentials at our level of theory. The disagreement between the experimental and the calculated potential values for CO formation is due to the inability of PBE to accurately determine the gas phase energies of CO and CO_2,[49] which would require a higher level of theory beyond the scope of the present work.

Numerous mechanisms have been proposed in the literature for electroreduction of CO_2,[7] all involving the activation of CO_2 via adsorption to the catalyst surface as the first step. In this work, we adopt a mechanism comprising of the following elementary reaction steps for the conversion of CO_2 into HCOOH and CO

1. $CO_2 + * \rightarrow CO_2^*$

2a. $CO_2^* + (H^+ + e^-) \rightarrow COOH^*$

2b. $CO_2^* + (H^+ + e^-) \rightarrow OCHO^*$

2c. $COOH^* \rightarrow CO^* + OH^*$

3a. $COOH^*/OCHO^* + (H^+ + e^-) \rightarrow HCOOH^*$

3b. $CO^* + OH^* + (H^+ + e^-) \rightarrow CO^* + H_2O^*$

4a. $HCOOH^* \rightarrow * + HCOOH$

4b. $CO^* + H_2O^* \rightarrow CO^* + H_2O$

4c. $CO^* + H_2O \rightarrow * + CO + H_2O$

where the species with asterisk (*) are adsorbed on the surface while those without are in the gas phase. The first step is a formally chemical transformation involving adsorption of CO_2 to the catalytically active site denoted by *. It is worth-mentioning that in the GC-DFT framework, chemical steps can also exhibit potential dependence, as has been found for CO_2 adsorption on metallic surfaces[50] or O_2 desorption from CoOOH.[51] CO_2 adsorption is followed by the first proton-coupled-electron-transfer (PCET) electrochemical step, resulting in two distinct intermediates, carboxyl ($COOH^*$, step 2a) or formyl ($OCHO^*$, step 2b). Either of these intermediates can undergo a second PCET step to yield adsorbed formic acid $HCOOH^*$ (step 3a), which can subsequently desorb in another chemical step (step 4a) to complete the catalytic cycle. On the other hand, carboxyl intermediate is susceptible to $C-O$ bond scission leading to (co-)adsorbed CO^* and OH^* species (step 2c). A second PCET step on OH^* could result in (co-)adsorbed water, H_2O^* (step 3b.) which can desorb into gaseous H_2O in a chemical step leaving behind CO^* on the surface (step 4b.). CO^*, in turn, can either desorb (step 4c) to complete the catalytic cycle or undergo further reduction reactions. This latter possibility is beyond the scope of the current investigation.

Since adsorption of CO_2 is a crucial first step which initiates the mechanism, we have studied it in detail as described in the following section. Fortunately, our grand-canonical approach is well-suited for in-depth exploration of this chemical transformation which has been mostly

overlooked in previous theoretical studies employing the standard CHE approach which can only tackle the electrochemical steps.[23,28]

3.2.1 Activation of CO_2 via adsorption

Activation of a free CO_2 molecule - via addition of a single electron to the high-lying LUMO, located mainly on electrophilic C - requires prohibitively strong reducing potential,

$$CO_2 + e^- \rightarrow CO_2^{\cdot -} \qquad E^0 = -1.49\ V \ \text{ vs. SHE}, \tag{4}$$

where $CO_2^{\cdot -}$ is highly active anionic radical with a bent shape caused by the repulsion between the added electron and the lone pairs on the two O atoms.[7,52] However, CO_2 can be activated via adsorption to a suitable catalyst surface, resulting in partially charged $CO_2^{\delta \cdot -}$ surface species, at milder reducing potentials. Adsorption of CO_2 could occur via an O (mono- or bidentate), C or mixed C−O mode;[53] however, in $CO_2^{\delta \cdot -}$ form, the O mode is rare as the resulting radical is predominantly located on C. Of course, as a neutral species, CO_2 could more easily adsorb through one of its O atoms without loosing its linearity.

Building on the results of the previous section, adsorption of CO_2 on Mo/S-edge was studied as a function of H coverage. For the remainder of the text, we will call CO_2 *activated* if its adsorption energy ΔG_{ads}^{nH}, represented as the free energy change of the following reaction, is exergonic; and adsorption leads to a bending of the CO_2 species (as opposed to a monodentate adsorption via O which does not result in the loss of linearity of the molecule):

$$nH^* + CO_2 \rightarrow \left(nH^*; CO_2^*\right), \tag{5}$$

where nH^* is the most stable configuration with n H atoms adsorbed on the given edge and $\left(nH^*; CO_2^*\right)$ is the corresponding most stable, coadsorbed configuration with one CO_2

molecule adsorbed on the same edge. Thus, ΔG_{ads}^{nH} can be written as,

$$\Delta G_{ads}^{nH} = G_{(nH^*;CO_2^*)}(U) - G_{nH^*}(U) - G_{CO_2} \quad (6)$$

where the first two quantities on the r.h.s are potential-dependent, GC free energies of the two configurations described above and G_{CO_2} is the gas-phase free energy of CO_2 calculated as described in the Methods section.

In Figure 3, we plot ΔG_{ads}^{nH} on S-edge as a function of electrode potential for three relevant H coverages (see Figures S8 and S9 for a detailed analysis of different H coverages and different CO_2 adsorption modes). In its most stable form, CO_2^* binds to two neighboring Mo atoms through a mixed C−O adsorption mode. One of the O atoms points away from the surface, rendering $CO_2{}^*$ a bent geometry with an angle of $\measuredangle OCO \approx 130°$, which signifies its activation with respect to the gas phase. Reconstruction of the edge is also observed whereby an S atom (highlighted with a pink circle in Figure 3) is displaced from its most-stable zigzag configuration. The first and second H atoms preferred to adsorb closer to the CO_2 molecule; the fourth H for 0.5 ML was most stable on the S atom nearest to the adsorbed CO_2 (Figure 3), vastly different from the most-stable 0.5 ML H configuration in the absence of CO_2 (Figure S3(a)). Notably, increasing H coverage does not induce any significant changes in the adsorption mode of CO_2.

As an important corollary, adsorption of CO_2 is affected by both the electrode potential and H coverage. For the case of 0.0 ML H (which is not stable in a wide range of electroreduction conditions), activation of CO_2 is endergonic. A significant effect of the electrode potential is nevertheless observed which originates from a partial charge transfer to CO_2^*. At 0.375 ML coverage, optimal adsorption is achieved and ΔG_{ads}^{nH} becomes negative below 0.07 V, which is substantially less than -1.49 V required for activation of a free CO_2 molecule.

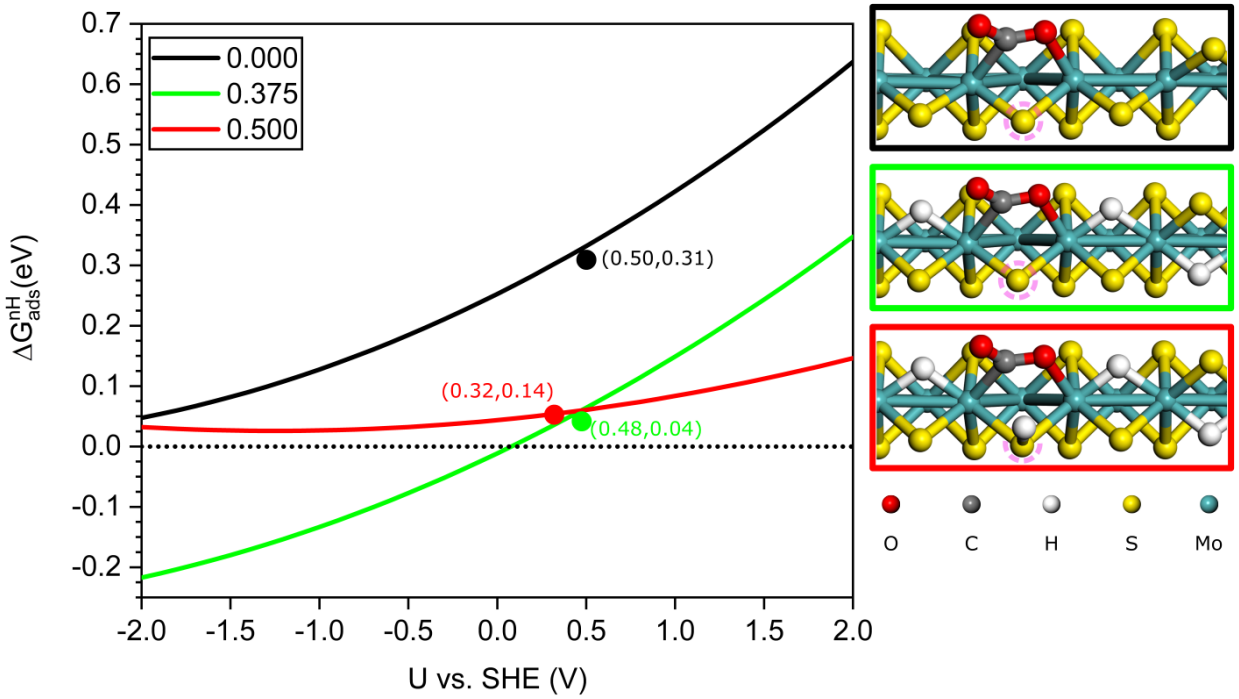

Figure 3: Free energy change of adsorption of CO_2 on S-edge of MoS_2 as a function of electrode potential and coverage of H. The circles correspond to the potential-of-zero charge (of coadsorbed $\left(nH^*; CO_2^*\right)$ system) and the corresponding free energy change of adsorption considering only neutral systems. The green curve crosses 0.0 eV at 0.07 V.

Compared to 0.0 ML, the effect of electrode potential is stronger at 0.375 ML hinting at a more favorable (partial) charge transfer at this coverage. Furthermore, 0.375 ML is also an optimal coverage as it induces least reconstruction to the S-edge upon adsorption of a CO_2 molecule (Figure S10). Increasing the coverage further to 0.5 ML, which is potentially the maximum equilibrium coverage on S-edge, CO_2 adsorption becomes unfavorable and has a very small dependence on the electrode potential as indicated by the nearly flat red curve in Figure 3. This can be attributed to the significant displacement of the 4^{th} H atom from its most-stable Mo−H−Mo adsorption mode to S−H mode which, in turn, is indispensable to accommodate CO_2^*. The Bader charge analysis (Table S1) reveals the expected charging of the adsorbed CO_2 species w.r.t the gas phase. Approximately 0.80 electrons are transferred from the surface, predominantly from topmost Mo atoms, to CO_2^* moieties ($\sim$ 0.7 of them are stabilized on C atom), irrespective of the H coverage. The H coverage, how-

ever, brings about a complementary charge redistribution whereby the Mo−H−Mo hydride species extract charge from topmost Mo atoms rendering them more electropositive which enables a stronger adsorption with more electronegative O atom. The electrode potential (see Table S1, 0.375 ML CO_2^* charged column), in turn, helps the catalyst surface recover its electronic density which is lost to CO_2^* and H^* species, making the overall coadsorbed system more stable. It is worth mentioning that the potential of zero charge and the corresponding adsorption free energies (shown by the filled circles in Figure 3 and S8) are significantly different from 0 V. Therefore, to study the chemical step of CO_2 adsorption, one really needs to explicitly account for the electrode potential and the often used CHE[21] approach involving solely zero-charge calculations will not be able to capture these effects.

We also investigated the effect of CO_2 adsorption on the competing HER. The overall trends of Volmer and Heyrovsky reaction energies are similar as without CO_2 adsorption. However, we find that up to 0.375 ML H coverage, the coadsorption of CO_2 favors the Volmer step but disfavors the Heyrovsky step i.e. S-edge has stronger tendency to accumulate H when CO_2 is adsorbed on the surface (Figure S11). Conversely, at 0.5 ML coverage the Heyrovsky step becomes more favored. This observation hints at potential blocking of HER by CO_2 adsorption and, indirectly, corroborates the optimal 0.375 ML H coverage required for CO_2 activation.

Moreover, we also studied the adsorption of CO_2 on Mo-edge at 0.0 ML H coverage, the predicted steady-state H coverage on this edge at electrode potentials relevant for CO_2 reduction. Two distinct adsorption modes were identified which are shown in Figure S12 along with their free energy change of adsorption. Unlike the situation on S-edge, neither of these adsorption modes is able to activate CO_2. At mild reducing potentials, the bridging Mo−S is the preferred adsorption mode, mainly because it causes very little reconstruction of the edge atoms and precludes unfavorable repulsive lateral interactions between O and S. The

Mo-Mo adsorption mode requires considerable edge reconstruction via formation of a S−S dimer moiety which can only be stabilized at very strong reducing potentials. Since, according to Eq. 4, CO_2 could undergo reduction even in solution starting from $\sim$ -1.5 V, the reactivity at very strongly reducing potentials is of limited relevance. Furthermore, unlike the situation on the S-edge, coadsorption of H was found to disfavor the adsorption of CO_2 on Mo-edge.

In conclusion for this section, the S-edge is shown to adsorb and activate CO_2 at potentials $<$ 0.0 V vs SHE. An optimal coverage of coadsorbed H was found key for CO_2 activation to take place, the Mo-edge is not able to adsorb or activate CO_2. This means that the subsequent steps for CO_2 reduction on Mo-edge are either far less prominent (remaining endergonic at any potential) or they occur in a different way, as studied in what follows.

3.2.2 Reactivity of S-edge

In the previous section, we demonstrated that 0.375 ML is the optimal H coverage for CO_2 adsorption which, in turn, initiates its activation through bending. Therefore, we investigate in the following the reduction process of CO_2 at this coverage by studying all reaction intermediates (RIs) in coadsorption with 0.375 ML H. The obtained free-energy reaction profile is illustrated in Figure 4 along with the most-stable adsorption modes of RIs; the constructed profile is based on the fitted GC free energies of the RIs given in Figure S16. As a reference to compare with the realistic H-covered case, we also studied the reaction profile on bare S-edge (Figure S14). Furthermore, the reaction profile in Figure 4 is plotted for two potentials, which represent the minimum potentials at which all the PCETs are exergonic or thermoneutral. The adsorbed CO_2^* is common to both HCOOH/CO formation and is exergonic at the two potentials highlighted. We recall that from -0.34 V to -0.54 V we observe very little change in the stability of CO_2^*, far less than the uncertainty associated with the DFT-based treatment adopted in this work. Therefore, a higher level of theory (e.g.

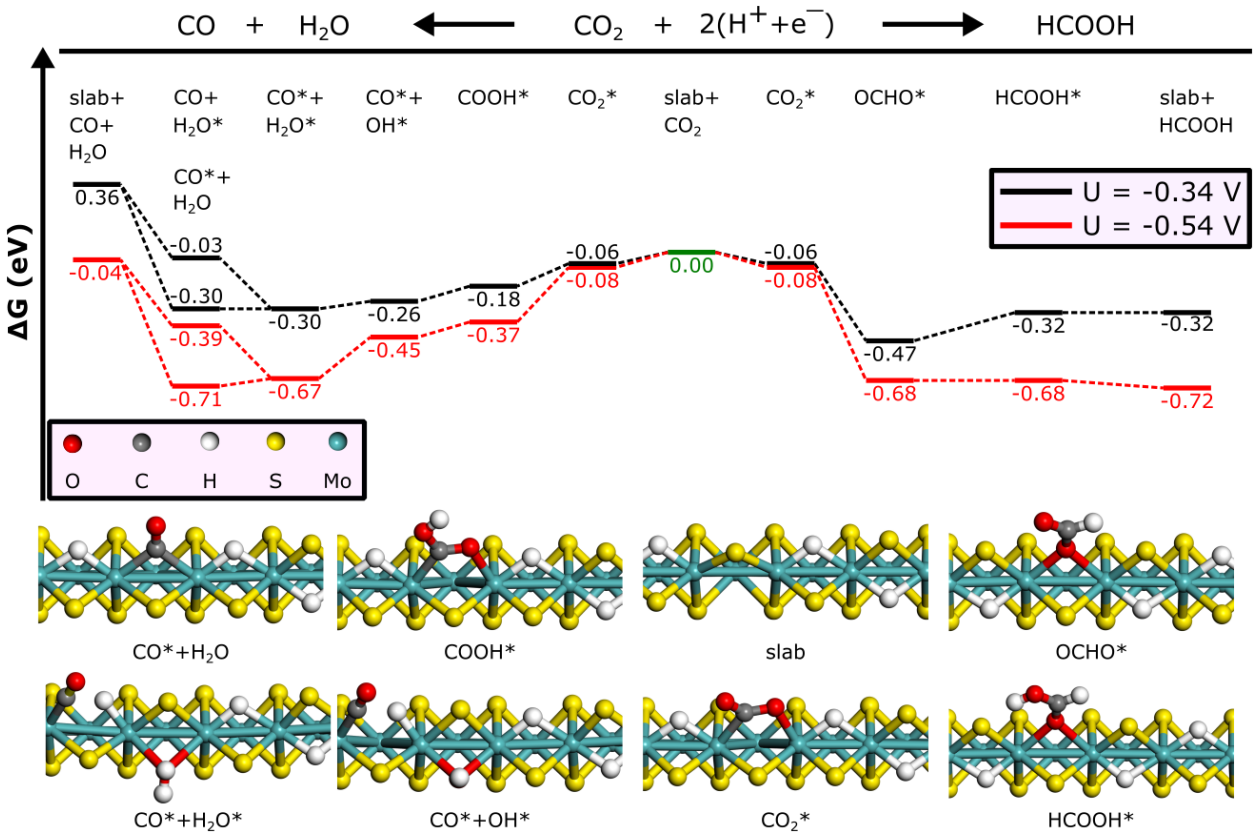

Figure 4: Free energy profile for the transformation of CO_2 into HCOOH (rightward from center) and CO (leftward from center) on 0.375 ML H covered S-edge for two reducing electrode potentials. The optimized geometries for the reaction intermediates have also been provided.

GC-RPA[54]) should be employed to make more accurate predictions of the effect of electrode potential on this chemical step. Since this first step is always exergonic and, therefore, has no limitation on the choice of the electrochemical potential, the latter is, in turn, determined by the stability of the RIs resulting from the subsequent PCETs.

Following CO_2^*, the first PCET event can produce formyl intermediate which, subsequently, exclusively forms formic acid and is, therefore, shown on the side of HCOOH in the reaction profile. Alternatively, carboxyl intermediate can also be formed which could convert into either HCOOH or CO. Although, transformation leading to either of these RIs is exergonic, even at mildly reducing -0.34 V, $COOH^*$ was found to be less stable than $OCHO^*$ by 0.29 eV (0.31 eV) at -0.34 V (-0.54 V). Therefore, we believe that carboxyl is mainly part of the CO pathway and is shown as such in the reaction profile. In its most stable state, $OCHO^*$ adsorbs via O between two Mo atoms with 3 coadsorbed H's in their most-stable Mo−H−Mo positions. Starting from $CO_2{}^*$, this adsorption mode would require a significant rearrangement of surface atoms and reaction species which could raise kinetic limitations on this transformation to formyl. In contrast, $COOH^*$ adsorbs in a mode very similar to $CO_2{}^*$ and could, therefore, be kinetically more accessible, even though it is thermodynamically less likely. Moreover, despite the substantial difference in relative stability between $OCHO^*$ and $COOH^*$, both species exhibit a stabilization of approximately -0.2 eV (consistent with a PCET) within the range of two potentials chosen. The free energy change associated with the first PCET is -0.47 eV (-0.68 eV) towards $OCHO^*$ and -0.18 eV (-0.37 eV) towards $COOH^*$ at mild (high) reducing potentials, respectively. Notably, similarly to HER on S-edge, we find that a Heyrovksy-like mechanism is favored over a Tafel-like mechanism: protons from the solution take part in the PCET instead of the H's adsorbed on the surface. This aligns with the inherent tendency of the S-edge to retain hydrogen on the Mo sites, subsequently rendering the edge Mo atoms more electropositive, (as it was shown previously through Bader-charge analysis, Table S1). This enhanced electropositivity leads to a more robust

adsorption of all RIs. The diminished stability of these two RIs on the bare S-edge (Figure S14) further attests to the heightened adsorption strength in the presence of coadsorbed H.

Starting from formyl, a second, Heyrovsky-like PCET leads to the formation of $HCOOH^*$ with free energy change of 0.15 eV and 0.0 eV at mildly and highly reducing potentials, respectively. As such, this step limits the choice of the potential towards the formation of HCOOH and only becomes thermoneutral at highly reducing -0.54 V. $HCOOH^*$ binds strongly to the surface in a configuration similar to $OCHO^*$. However, $HCOOH^*$ experiences a stronger effect of the increase in the reducing potential (-0.36 eV stabilization in going from -0.34 V to -0.54 V, again in agreement with a PCET mechanism). Exergonic desorption of $HCOOH^*$ into gaseous HCOOH completes the catalytic cycle to the formation of formic acid and recovers the initial catalyst with the corresponding 0.375 ML H coverage. The free energy change of desorption becomes slightly more exergonic at highly reducing potential.

On the other hand, pathway to CO formation is opened when $COOH^*$ is dissociated to form CO^* and OH^* in a chemical step. We find that this chemical transformation is exergonic on S-edge, and it displays a very weak dependence on the electrode potential (Figure S17). Notably, we consider the coadsorbed structure CO^*+OH^* where CO^* binds to a Mo atom via C, and is slightly tilted towards Mo−Mo edge displacing one of the H's from its most stable Mo−H−Mo configuration, and OH^* binds in *trans* fashion to the neighboring Mo−Mo edge via O with H pointing vertically upward. This coadsorbed configuration experiences the expected ≈ -0.20 eV stability increase in going from -0.34 to -0.54 V.

In this coadsorbed configuration, the second PCET event likely leads to the formation of a CO^*+H_2O^* configuration with free energy changes of -0.04 eV (-0.22 eV) at mild (high) reducing potentials. Similar to $HCOOH^*$, this configuration is highly influenced by the

electrode potential, showing a significant -0.37 eV increase in stability from in the chosen potential range. On the one hand, adsorbed H_2O^* may contribute to H_2 evolution (Figure S18) via mechanisms previously discussed in literature,[55] necessitating its immediate desorption. However, unlike $HCOOH^*$, the desorption processes of H_2O^* and CO^* are complex. Analyzing the reaction profile (Figure 4) reveals exergonic H_2O^* desorption only at potentials more reducing than -0.34. Importantly, this contrasts with the bare S-edge, where H_2O^* desorption is consistently endergonic (Figure S14). Furthermore, H_2O^* desorption becomes endergonic at all potentials if CO^* has already been desorbed, indicating strong lateral interactions between these coadsorbed species. Thus, desorption of H_2O^* could be a limiting step towards formation of CO.

Desorption of CO^* into gaseous CO was determined to be endothermic (0.27 eV) with no discernible impact of the electrode potential. The desorption process becomes noticeably more challenging (0.66 eV) when H_2O^* has already desorbed, underscoring the existence of repulsive lateral interactions between H_2O^* and CO^*. This observation suggests that the desorption of CO^* might involve a more intricate mechanism, potentially linked to a higher coverage induced by its facile diffusion on the catalyst surface, as discussed in Ref.[56] and briefly outlined in the SI. Alternatively, and with great potential benefit, it could undergo further conversion into more reduced products such as formaldehyde, methane, and methanol. However, exploring this latter aspect is beyond the scope of the current study.

3.2.3 Reactivity of Mo-edge

As shown previously, Mo-edge is very active for HER, thanks to a very exergonic Heyrovsky step, at CO_2 reducing potentials and thus displays an equilibrium coverage of 0.0 ML under steady-state conditions. Therefore, we study the reactivity of bare Mo-edge for which the resulting reaction free energy profile is illustrated in Figure 5 at -0.80 V, which corresponds to the potential at which the first PCET to either of the formyl or hydroxyl intermediates

is exergonic; the corresponding fitted curves of GC free energy are given in Figure S15.

As demonstrated above, CO_2 activation via adsorption is not possible on Mo-edge, in-

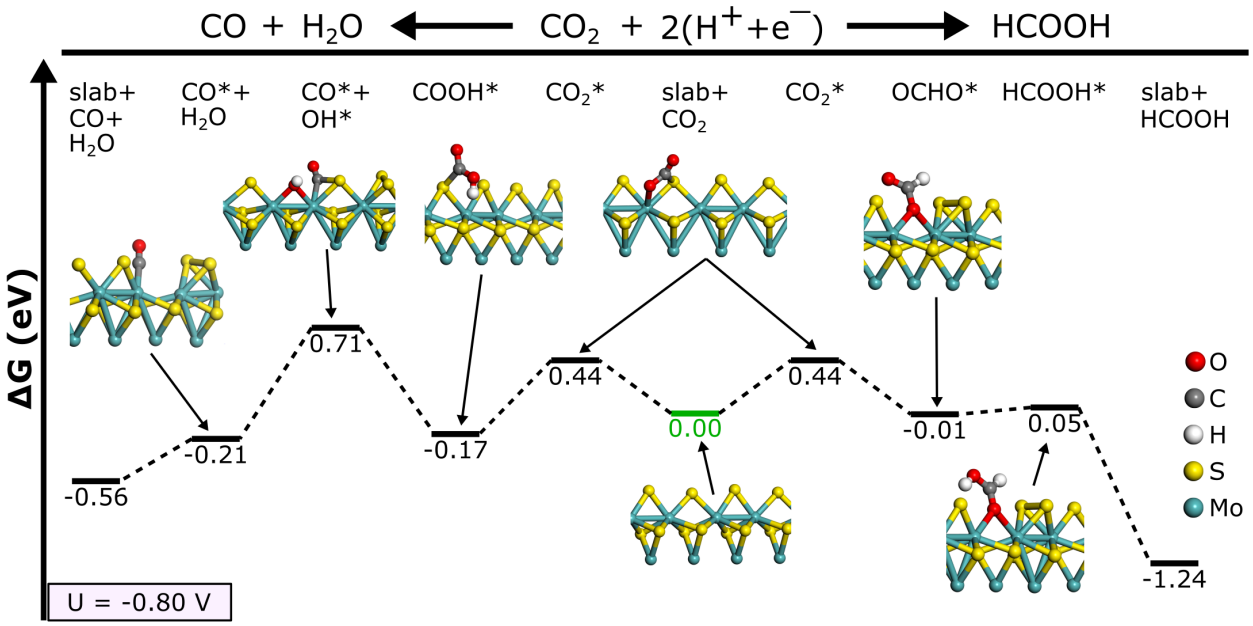

Figure 5: Free energy profile for reduction of CO_2 into HCOOH (rightward from center) and CO (leftward from center) on bare Mo-edge at -0.8 V.

dicated by its very endergonic 0.44 eV free energy change of adsorption on this edge. This, combined with the fact that Mo-edge has 0.0 ML H coverage, necessitates the assumption of a concerted mechanism whereby adsorption of CO_2 and first PCET take place simultaneously, making it a noteworthy distinction compared to the behavior observed on the S-edge. This combined mechanism is anticipated to involve higher kinetic barriers, and is more challenging to envision since the CO_2-proton interaction in the solvent must coincide with the arrival of an electron at the surface. On the S-edge, the adsorbed CO_2^* is activated and already in proximity to both the incoming surface electron and the incoming solvent proton. It is important to highlight that the majority of previous DFT studies utilizing the standard CHE approach assume the prevalence of the former scenario.[23,28]

The first PCET RIs $COOH^*$ and $OCHO^*$, exhibit very diminished stability on Mo-edge,

compared to S-edge, as signified by relatively flat zone of reaction profile around the reference state in Figure 5. Interestingly, $COOH^*$ is slightly more stable than $OCHO^*$, in contrast with the behavior on S-edge. This is possibly because $COOH^*$ has a monodentate C−S adsorption mode which requires no reconstruction of the edge; adsorption of $OCHO^*$, on the other hand, requires formation of a S−S dimer to accommodate its bidentate Mo−O−Mo mode.

Since the two RIs show similar stability on this edge, they can both result in HCOOH following a second PCET step. The adsorbed state $HCOOH^*$ shows little stability on this edge and thus the free energy change of desorption of $HCOOH^*$ is very exergonic. This hints at a possible concerted desorption mechanism whereby second PCET is combined with simultaneous desorption of the resulting product. This could particularly be the case starting from $COOH^*$ as it would have to undergo a considerable rearrangement from its C−S adsorption mode to yield bidentate adsorbed $HCOOH^*$. Instead, it could directly desorb into HCOOH following a second PCET with a free energy change of desorption of $\approx$ -1.04 eV at -0.8 V. Similar to S-edge, the free energy change of desorption of HCOOH shows a weak potential dependence.

Dissociation of $COOH^*$ leading to the formation of CO^*+OH^* is highly endergonic due to the inability of highly coordinated (sixfold) Mo atoms on this edge to stabilize the resulting coadsorbed structure. The most stable coadsorbed configuration has CO^* adsorbed in bridged Mo−S mode and OH^* adsorbed on Mo−Mo bridge position, similar to the adsorption behavior of S−H moieties on this edge. However, if desorption of H_2O is combined with the second PCET step, as done in various studies in literature,[23,28] the overall transformation from $COOH^*$ to CO^* becomes exergonic. In contrast to the S-edge, where they have comparable stability, CO^* is slightly more stable on the Mo-edge compared to $HCOOH^*$. Nevertheless, CO^* is very weakly adsorbed on this edge thus enabling its exergonic desorption

and, potentially, opening the path to the production of CO. However, a mere thermodynamic analysis is very limited in this context, and one needs to perform detailed kinetic analysis (most likely employing biased molecular dynamics simulations using explicit electrolyte) to understand the activation energies of such coupled elementary reaction steps.

Finally, it is worth mentioning that the thermodynamically stable S coverage of this edge is expected to vary under reaction conditions via release of H_2S.[28] At lower S coverage, activation of CO_2 via adsorption on unsaturated Mo atoms, and even stronger adsorption of CO^*, is highly likely, which would impact the reactivity. However, this investigation is beyond the scope of the current study as it would require evaluating the kinetic barrier for H_2S release which is suspected to increase when the S-coverage decrease.

4 Conclusion

By means of the grand-canonical DFT calculations, we have investigated the edge state and the resulting reactivity of partially-sulfided Mo-/S-edge of MoS_2 for photocatalytic or electrocatalytic reduction of CO_2. Our analysis unveils distinct steady-state H coverages on the two edges, stemming from the differing degree of competition between Volmer adsorption and Heyrovsky desorption steps. The S-edge was observed to contain strongly-adsorbed hydride species at bridging Mo sites, which exhibited reduced propensity for hydrogen evolution via the Heyrovsky mechanism, resulting in an equilibrium H coverage ranging from 0.375 to 0.5 ML. In contrast, the Mo-edge exhibited a very small, possibly 0 ML, steady-state H coverage attributed mainly to highly exergonic Heyrovsky step which evolves the less stable H^* species, present predominantly as S−H moieties, found on this edge. In terms of reactivity, 0.375 ML H-covered S-edge allows optimal CO_2 adsorption with negative ΔG_{ads} for negative electrode potentials vs SHE. The adsorption occurs in a mixed C−O bidentate mode on two neighboring Mo sites, and the resulting CO_2^* species is partially (negatively) charged due to

favorable electron transfer from the surface and has bent shape, signifying activation of CO_2. As a result of this activation of CO_2, pathway to either of the two-electron products - CO^* or HCOOH - is opened with limiting potentials of -0.34 V and -0.54 V, respectively. Along the reaction coordinate, $OCHO^*$ intermediate leading to HCOOH was ≈ 0.3 eV more stable than $COOH^*$, the former, however. suffers from a potential limiting second PCET towards formation of adsorbed $HCOOH^*$. Conversely, $C-O$ bond-dissociation in $COOH^*$ is exergonic even at less reducing potentials and the coadsorbed $CO^* + OH^*$ configuration undergoes exergonic PCET to yield $CO^* + H_2O^*$ state which is only 0.1 eV less stable than $HCOOH^*$ state. Therefore, one can not rule out the possible formation of CO^* on this edge. Furthermore, the desorption of CO^* was endergonic on the S-edge, indicating that it might be further reduced to other C_1 products such as methanol or methane. The S-edge was found to be very active for HER at electrode potentials close to 0 V. However, at reducing potentials involved in CO_2 reduction, HER was potentially hindered by the presence of competing carbonaceous species on the surface. On the Mo-edge, the adsorption of CO_2 is endergonic (0.44 eV). However, assuming concerted PCET+adsorption/desorption elementary steps, HCOOH was determined to be the major product on this edge. This was also corroborated by the fact that the $C-O$ bond-dissociation involved in CO formation is strongly endergonic on this edge making this pathway highly unlikely.

Overall, we find that MoS_2 particles exposing the considered S-edge should be an active photo-electro-catalyst for CO_2 to formic acid reduction at mild reducing potentials. At strong reducing potentials, CO might also be formed, which suffers from an endergonic desorption and, therefore, is expected to be further reduced, a possibility which will be the subject of a forthcoming work. In contrast, the Mo-edge seems to be less favorable for CO_2 reduction unless mechanisms that combine the proton-electron transfer and the adsorption/desorption of CO_2/products are operative. Such complex events would presumably encounter high activation free energies and need to be further investigated by simulating

kinetics, explicit-solvent, for instance by including molecular-dynamics approaches.

Acknowledgement

This work is part of the "RatiOnAl Design for CATalysis" (ROAD4CAT) industrial chair, project IDEXLYON funded by the French National Research Agency (ANR-16-IDEX-0005) and the Commissariat-General for Investment (CGI) within the framework of Investissements d'Avenir program ("Investment for the future"). The authors thank the SYSPROD project and AXELERA Pôle de Compétitivité for financial support (PSMN Data Center). Calculations were performed using HPC resources (Jean Zay and Irene) from GENCI-CINES (Grant A0140806134) and ENER 440 from IFP Energies nouvelles.

Supporting Information Available

The Supporting Information is available free of charge at `https://pubs.acs.org/doi/10.1021/xxx` Additional Figures, Tables and discussion related to hydrogenation of the two edges; CO_2 adsorption and the corresponding Bader charge analysis; reaction free energy profile on bare S-edge and CO desorption (PDF). The optimized coordinates of all symmetric, zero-charge systems investigated herein are freely available at the open-source Nomad database under: `https://dx.doi.org/10.17172/NOMAD/2024.02.06-1`.

References

(1) Beller, M.; Centi, G.; Sun, L. Chemistry Future: Priorities and Opportunities from the Sustainability Perspective. *ChemSusChem* **2017**, *10*, 6–13.

(2) Lanzafame, P.; Abate, S.; Ampelli, C.; Genovese, C.; Passalacqua, R.; Centi, G.; Perathoner, S. Beyond Solar Fuels: Renewable Energy-Driven Chemistry. *ChemSusChem* **2017**, *10*, 4409–4419.

(3) Navarrete, A.; Centi, G.; Bogaerts, A.; Martín, Á.; York, A.; Stefanidis, G. D. Harvesting Renewable Energy for Carbon Dioxide Catalysis. *Energy Technology* **2017**, *5*, 796–811.

(4) Vincenzo Barbarossa; Giuseppina Vanga; Rosanna Viscardi; Daniele Mirabile Gattia CO_2 as Carbon Source for Fuel Synthesis. *Energy Procedia* **2014**, *45*, 1325–1329.

(5) Hori, Y. In *Modern Aspects of Electrochemistry*; Vayenas, C. G., White, R. E., Gamboa-Aldeco, M. E., Eds.; Springer New York: New York, NY, 2008; pp 89–189.

(6) Yaru Lei; Zheng Wang; Ai Bao; Xiaolong Tang; Xiubing Huang; Honghong Yi; Shunzheng Zhao; Ting Sun; Junyi Wang; Fengyu Gao Recent advances on electrocatalytic CO_2 reduction to resources: Target products, reaction pathways and typical catalysts. *Chemical Engineering Journal* **2023**, *453*, 139663.

(7) Wang, Y.; Chen, E.; Tang, J. Insight on Reaction Pathways of Photocatalytic CO_2 Conversion. *ACS catalysis* **2022**, *12*, 7300–7316.

(8) Habisreutinger, S. N.; Schmidt-Mende, L.; Stolarczyk, J. K. Photocatalytic Reduction of CO_2 on TiO_2 and Other Semiconductors. *Angewandte Chemie International Edition* **2013**, *52*, 7372–7408.

(9) Barber, J.; Tran, P. D. From natural to artificial photosynthesis. *Journal of the Royal Society, Interface* **2013**, *10*, 20120984.

(10) Dogutan, D. K.; Nocera, D. G. Artificial Photosynthesis at Efficiencies Greatly Exceeding That of Natural Photosynthesis. *Accounts of Chemical Research* **2019**, *52*, 3143–3148.

(11) Ruinart de Brimont, M.; Dupont, C.; Daudin, A.; Geantet, C.; Raybaud, P. Deoxygenation mechanisms on Ni-promoted MoS_2 bulk catalysts: A combined experimental and theoretical study. *Journal of Catalysis* **2012**, *286*, 153–164.

(12) Hervé, T., Pascal, R., Eds. *CATALYSIS BY TRANSITION METAL SULPHIDES. From Molecular Theory to Industrial Application.*; Editions TECHNIP: Paris, 2013.

(13) Hinnemann, B.; Moses, P. G.; Bonde, J.; Jørgensen, K. P.; Nielsen, J. H.; Horch, S.; Chorkendorff, I.; Nørskov, J. K. Biomimetic Hydrogen Evolution: MoS_2 Nanoparticles as Catalyst for Hydrogen Evolution. *Journal of the American Chemical Society* **2005**, *127*, 5308–5309.

(14) Thomas F. Jaramillo; Kristina P. Jørgensen; Jacob Bonde; Jane H. Nielsen; Sebastian Horch; Ib Chorkendorff Identification of Active Edge Sites for Electrochemical H_2 Evolution from MoS_2 Nanocatalysts. *Science (New York, N.Y.)* **2007**, *317*, 100–102.

(15) Balan, B.; Xavier, M. M.; Mathew, S. MoS_2-Based Nanocomposites for Photocatalytic Hydrogen Evolution and Carbon Dioxide Reduction. *ACS Omega* **2023**, *8*, 25649–25673.

(16) Singh, S.; Modak, A.; Pant, K. K.; Sinhamahapatra, A.; Biswas, P. MoS_2–Nanosheets-Based Catalysts for Photocatalytic CO_2 Reduction: A Review. *ACS Applied Nano Materials* **2021**, *4*, 8644–8667.

(17) Asadi, M.; Kumar, B.; Behranginia, A.; Rosen, B. A.; Baskin, A.; Repnin, N.; Pisasale, D.; Phillips, P.; Zhu, W.; Haasch, R. et al. Robust carbon dioxide reduction on molybdenum disulphide edges. *Nature communications* **2014**, *5*, 4470.

(18) Brian A. Rosen; Amin Salehi-Khojin; Michael R. Thorson; Wei Zhu; Devin T. Whipple; Paul J. A. Kenis; Richard I. Masel Ionic Liquid–Mediated Selective Conversion of CO_2 to CO at Low Overpotentials. *Science* **2011**, *334*, 643–644.

(19) Favre, R.; Raybaud, P.; Le Bahers, T. Electronic structures of the MoS_2/TiO_2 (anatase) heterojunction: influence of physical and chemical modifications at the 2D- or 1D-interfaces. *Phys. Chem. Chem. Phys.* **2022**, *24*, 2646–2655.

(20) Hezam, A.; Alkanad, K.; Bajiri, M. A.; Strunk, J.; Takahashi, K.; Drmosh, Q. A.; Al-Zaqri, N.; Krishnappagowda, L. N. 2D/1D MoS_2/TiO_2 Heterostructure Photocatalyst with a Switchable CO_2 Reduction Product. *Small methods* **2023**, *7*, e2201103.

(21) Nørskov, J. K.; Rossmeisl, J.; Logadottir, A.; Lindqvist, L.; Kitchin, J. R.; Bligaard, T.; Jónsson, H. Origin of the Overpotential for Oxygen Reduction at a Fuel-Cell Cathode. *The Journal of Physical Chemistry B* **2004**, *108*, 17886–17892.

(22) Peterson, A. A.; Abild-Pedersen, F.; Studt, F.; Rossmeisl, J.; Nørskov, J. K. How copper catalyzes the electroreduction of carbon dioxide into hydrocarbon fuels. *Energy Environ. Sci.* **2010**, *3*, 1311–1315.

(23) Chan, K.; Tsai, C.; Hansen, H. A.; Nørskov, J. K. Molybdenum Sulfides and Selenides as Possible Electrocatalysts for CO_2 Reduction. *ChemCatChem* **2014**, *6*, 1899–1905.

(24) Hong, X.; Chan, K.; Tsai, C.; Nørskov, J. K. How Doped MoS_2 Breaks Transition-Metal Scaling Relations for CO_2 Electrochemical Reduction. *ACS catalysis* **2016**, *6*, 4428–4437.

(25) Peterson, A. A.; Nørskov, J. K. Activity Descriptors for CO_2 Electroreduction to Methane on Transition-Metal Catalysts. *The Journal of Physical Chemistry Letters* **2012**, *3*, 251–258.

(26) Tsai, C.; Chan, K.; Nørskov, J. K.; Abild-Pedersen, F. Understanding the Reactivity of Layered Transition-Metal Sulfides: A Single Electronic Descriptor for Structure and Adsorption. *The Journal of Physical Chemistry Letters* **2014**, *5*, 3884–3889.

(27) Mao, X.; Wang, L.; Xu, Y.; Li, Y. Modulating the MoS_2 Edge Structures by Doping Transition Metals for Electrocatalytic CO_2 Reduction. *The Journal of Physical Chemistry C* **2020**, *124*, 10523–10529.

(28) Pedersen, P. D.; Vegge, T.; Bligaard, T.; Hansen, H. A. Trends in CO 2 Reduction on Transition Metal Dichalcogenide Edges. *ACS catalysis* **2023**, *13*, 2341–2350.

(29) Zhao, Y.; Chen, Y.; Ou, P.; Song, J. Basal Plane Activation via Grain Boundaries in Monolayer MoS_2 for Carbon Dioxide Reduction. *ACS catalysis* **2023**, *13*, 12941–12951.

(30) Gattrell, M.; Gupta, N.; Co, A. A review of the aqueous electrochemical reduction of CO_2 to hydrocarbons at copper. *Journal of Electroanalytical Chemistry* **2006**, *594*, 1–19.

(31) Landers, A. T.; Fields, M.; Torelli, D. A.; Xiao, J.; Hellstern, T. R.; Francis, S. A.; Tsai, C.; Kibsgaard, J.; Lewis, N. S.; Chan, K. et al. The Predominance of Hydrogen Evolution on Transition Metal Sulfides and Phosphides under CO_2 Reduction Conditions: An Experimental and Theoretical Study. *ACS Energy Letters* **2018**, *3*, 1450–1457.

(32) Kresse, G.; Furthmüller, J. Efficient iterative schemes for ab initio total-energy calculations using a plane-wave basis set. *Phys. Rev. B* **1996**, *54*, 11169–11186, Publisher: American Physical Society.

(33) Perdew, J. P.; Burke, K.; Ernzerhof, M. Generalized Gradient Approximation Made Simple. *Phys. Rev. Lett.* **1996**, *77*, 3865–3868.

(34) Grimme, S.; Antony, J.; Ehrlich, S.; Krieg, H. A consistent and accurate ab initio parametrization of density functional dispersion correction (DFT-D) for the 94 elements H-Pu. *The Journal of Chemical Physics* **2010**, *132*, 154104.

(35) Grimme, S.; Ehrlich, S.; Goerigk, L. Effect of the damping function in dispersion corrected density functional theory. *Journal of Computational Chemistry* **2011**, *32*, 1456–1465.

(36) Blöchl, P. E. Projector augmented-wave method. *Phys. Rev. B* **1994**, *50*, 17953–17979.

(37) Kresse, G.; Joubert, D. From ultrasoft pseudopotentials to the projector augmented-wave method. *Phys. Rev. B* **1999**, *59*, 1758–1775.

(38) Ruffman, C.; Gordon, C. K.; Skúlason, E.; Garden, A. L. Mechanisms and Potential-Dependent Energy Barriers for Hydrogen Evolution on Supported MoS2 Catalysts. *The Journal of Physical Chemistry C* **2020**, *124*, 17015–17026.

(39) Raybaud, P.; Hafner, J.; Kresse, G.; Kasztelan, S.; Toulhoat, H. Ab Initio Study of the H_2–H_2S/MoS_2 Gas–Solid Interface: The Nature of the Catalytically Active Sites. *Journal of Catalysis* **2000**, *189*, 129–146.

(40) Taylor, C. D.; Wasileski, S. A.; Filhol, J.-S.; Neurock, M. First principles reaction modeling of the electrochemical interface: Consideration and calculation of a tunable surface potential from atomic and electronic structure. *Phys. Rev. B* **2006**, *73*, 165402.

(41) Abidi, N.; Bonduelle-Skrzypczak, A.; Steinmann, S. N. Revisiting the Active Sites at the MoS_2/H_2O Interface via Grand-Canonical DFT: The Role of Water Dissociation. *ACS Applied Materials & Interfaces* **2020**, *12*, 31401–31410, PMID: 32551477.

(42) Mathew, K.; Sundararaman, R.; Letchworth-Weaver, K.; Arias, T. A.; Hennig, R. G. Implicit solvation model for density-functional study of nanocrystal surfaces and reaction pathways. *J. Chem. Phys.* **2014**, *140*, 084106.

(43) Mathew, K.; Kolluru, V. S. C.; Mula, S.; Steinmann, S. N.; Hennig, R. G. Implicit self-consistent electrolyte model in plane-wave density-functional theory. *J. Chem. Phys.* **2019**, *151*, 234101.

(44) Mathew, K.; Kolluru, V. S. C.; Hennig, R. G. VASPsol: Implicit solvation and electrolyte model for density-functional theory. 2018; `https://github.com/henniggroup/VASPsol`, (Date Accessed: 2024-05-29).

(45) Deubel, D. V.; Lau, J. K.-C. In silico evolution of substrate selectivity: comparison of organometallic ruthenium complexes with the anticancer drug cisplatin. *Chem. Commun.* **2006**, 2451–2453.

(46) Kua, J.; Thrush, K. L. HCN, Formamidic Acid, and Formamide in Aqueous Solution: A Free-Energy Map. *The Journal of Physical Chemistry B* **2016**, *120*, 8175–8185.

(47) GoldBook, Standard Hydrogen electrode, Version 3.0.1. `http://goldbook.iupac.org/S05917.html`, (Date Accessed: 2024-05-29).

(48) Huang, Y.; Nielsen, R. J.; Goddard, W. A., III; Soriaga, M. P. The Reaction Mechanism with Free Energy Barriers for Electrochemical Dihydrogen Evolution on MoS_2. *Journal of the American Chemical Society* **2015**, *137*, 6692–6698.

(49) Granda-Marulanda, L. P.; Rendón-Calle, A.; Builes, S.; Illas, F.; Koper, M. T. M.; Calle-Vallejo, F. A Semiempirical Method to Detect and Correct DFT-Based Gas-Phase Errors and Its Application in Electrocatalysis. *ACS catalysis* **2020**, *10*, 6900–6907.

(50) Steinmann, S. N.; Michel, C.; Schwiedernoch, R.; Filhol, J.-S.; Sautet, P. Modeling the HCOOH/CO_2 Electrocatalytic Reaction: When Details Are Key. *ChemPhysChem* **2015**, *16*, 2307–2311.

(51) Curutchet, A.; Colinet, P.; Michel, C.; Steinmann, S. N.; Bahers, T. L. Two-sites are better than one: revisiting the OER mechanism on CoOOH by DFT with electrode polarization. *Phys. Chem. Chem. Phys.* **2020**, *22*, 7031–7038.

(52) H.-J. Freund; M.W. Roberts Surface chemistry of carbon dioxide. *Surface Science Reports* **1996**, *25*, 225–273.

(53) Chang, X.; Wang, T.; Gong, J. CO_2 photo-reduction: insights into CO_2 activation and reaction on surfaces of photocatalysts. *Energy & Environmental Science* **2016**, *9*, 2177–2196.

(54) Wei, Z.; Göltl, F.; Steinmann, S. N.; Sautet, P. Modeling Electrochemical Processes with Grand Canonical Treatment of Many-Body Perturbation Theory. *J. Phys. Chem. Lett.* **2022**, *13*, 6079–6084.

(55) Abidi, N.; Bonduelle-Skrzypczak, A.; Steinmann, S. N. Revisiting the Active Sites at the MoS_2/H_2O Interface via Grand-Canonical DFT: The Role of Water Dissociation. *ACS Applied Materials & Interfaces* **2020**, *12*, 31401–31410.

(56) Reaction mechanisms for reduction of CO_2 to CO on monolayer MoS_2. *Applied Surface Science* **2020**, *499*, 143964.

TOC Graphic